Small-Scale Vortex-Induced Vibration Wind Energy Harvesters

Written By:
Frank Ciliberto
Carly Neeld
Brooke Pierce
Ethan Shipulski

Advisor:
Brian Savilonis

March 22, 2019

Abstract

The goal of this project was to find innovative ways to harvest wind energy using phenomena known as vortex shedding and aeroelastic fluttering. We developed two vibrational small-scale wind energy harvesters, employing the use of a bluff body and an airfoil. We compared the theoretical natural and shedding frequencies to determine parameters for the spring constants in each system. Using an electromagnetic transducer, we harvested up to 1 milliwatt of power. We demonstrated the feasibility of our designs and explored the possibilities of scaling the system for use in different applications.

Table of Contents

List of Tables

List of Figures

Introduction

The development of the renewable energy industry has continued to grow throughout recent years due to the increase of carbon emitted by non-renewable resources. Large-scale wind and solar innovations are constantly being created and improved; however, there has been special attention given to small-scale devices. Small-scale energy harvesting has seen an increase in development due to its ability to be applied in remote locations. Proving the feasibility of small-scale applications gives engineers the ability to scale systems for larger-scale applications.

One of the most abundant and common resources of renewable energy is wind. Wind energy has a low impact on the environment and is one of the least expensive sources currently available. Wind energy provides about 8 percent of the energy generated in the U.S. (U.S., n.d.). Wind harvesting has two primary methods: rotational wind harvesting and oscillation wind harvesting. Although both methods utilize the conversion of wind energy to electrical energy, the mechanical principles behind each method are different. When selecting a wind harvesting method, it is important to consider the applications and the corresponding advantages and disadvantages.

A traditional wind turbine has rotating blades connected to a center shaft, which is connected to a gearbox. This sends the mechanical energy of the rotors to a generator and then converts the mechanical energy into electrical energy. Other wind turbines without gears have rotor blades that are directly connected to the generator, rotating a magnetic field at the same speed as the blades. An advantage of rotational wind harvesting is the area of wind turbine blades exceeds the area of the ground needed to install this device; therefore wind turbines maximize the available wind energy in a given area. However, due to their dimensions and positioning, they are limited by their proximity to airports, other infrastructure, and are a concern for wildlife. Overall, rotational wind-harvesting devices are effective and efficient at a larger scale, making them an ideal option for commercial applications.

Oscillation wind-harvesting devices make use of vortex-induced vibrations (VIV) to generate electricity. This occurs when a flow moves over a bluff body or an airfoil. As the flow moves over the bluff body or airfoil, an oscillating lift force occurs. This alternating motion

causes the bluff body or airfoil to oscillate. The benefits of VIV energy harvesters are that they have the capability to generate power in low wind speeds. These systems also have minimal impact on the environment. The use of small-scale VIV energy harvesters is currently a developing field that is looking to discover ways to harvest the energy to produce a larger energy density. Because of this, there is still a need for more research on how to create an efficient and effective small-scale VIV energy harvester.

The goal of this project was to construct two small-scale vibrating wind energy harvesters. The first prototype used a suspended bluff body attached to springs that vertically oscillated. The second prototype used a symmetrical airfoil that oscillated and fluttered in a horizontal direction along a track with springs. Both of these prototypes used an electromagnetic transducer to harvest energy.

Background

Vortex-Induced Vibrations Theory

Aeroelastic fluttering is a phenomenon that has been explored by engineers for decades. It involves the phenomenon of vortex shedding, resonance, instability, and physical elasticity. A common example of aeroelastic fluttering can be seen with airplane wings. When the resonant frequency is reached, the wing is flexed back and forth rapidly, causing fatigue stress, and potential failure. Although fluttering is generally a catastrophic force that engineers work to eliminate, it is possible to purposefully induce. In order to fully understand aeroelastic fluttering, it is important to understand what happens when there is a fluid flow over a bluff body. This includes shear stress, boundary layers, Reynolds number, and Strouhal number.

Shear stress in a fluid is a stress caused by a difference in flow velocities in two streamlines. When a fluid is flowing faster in one plane than another (in the same direction), the parallel forces create a shear stress.

Any object moving through a fluid, along with a stationary object that is experiencing fluid flow, has a boundary layer. Boundary layer flow is the tendency of the velocity to be zero at the surface where flow is taking place. The boundary layer is the area in which the flow transitions from zero velocity at the surface, to free stream velocity. Over a flat plate, the boundary layer thickness for a laminar flow can be found by using Equation 1.

$$\delta/x = 5/\sqrt{Re} \tag{1}$$

δ = *boundary layer thickness*

x = *distance from leading edge*

Re = *Reynolds number*

For a Reynolds number below 2300, the internal flow is considered laminar. Laminar flow is more orderly and is typically used for testing small-scale energy harvesters. For turbulent flow with a higher Reynolds number of 4000, a natural test could be conducted outdoors (Subramanian, n.d.). There are various equations to calculate the boundary layer thickness for

different shapes, and these thicknesses can also be calculated through numerical methods such as computational fluid dynamics (CFD).

A bluff body is an object that is located in a flow, that has substantial separated flow over the surface of the body (Bearman, n.d.). Flow separation is a condition in which the boundary layer flow over a body separates from the surface of the body. This effect creates a low-pressure area near the object, which creates an area of retrograde flow (flow in the opposite direction of the free stream velocity). If the Reynolds number stays low, the separated flow around a bluff body stays stable; however, as the Reynolds number rises, the flow tends to be uneven, and creates vortices and instabilities in the flow (Bearman, n.d.).

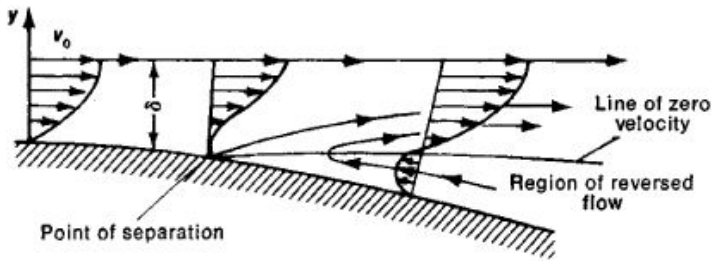

Figure 1: Flow separation at the point of separation (Bearman, n.d)

Separation of flow is the main driving force from which vortex shedding originates. The interaction between the separating layers, one of which has a forward velocity, and the other having a retrograde velocity, creates this vortex (Bearman, n.d.). Once the vortex is created, it is shed off of the downstream face of the bluff body, and the vortex travels downstream. Vortices are created and shed off the back of the bluff body, alternating the side they shed from. The alternating shedding of vortices creates a back-and-forth force on the bluff body. The vortices are also relatively stable after separating from the object, so they tend to create a "street" of vortices downstream of the object, sometimes called the Karman vortex street.

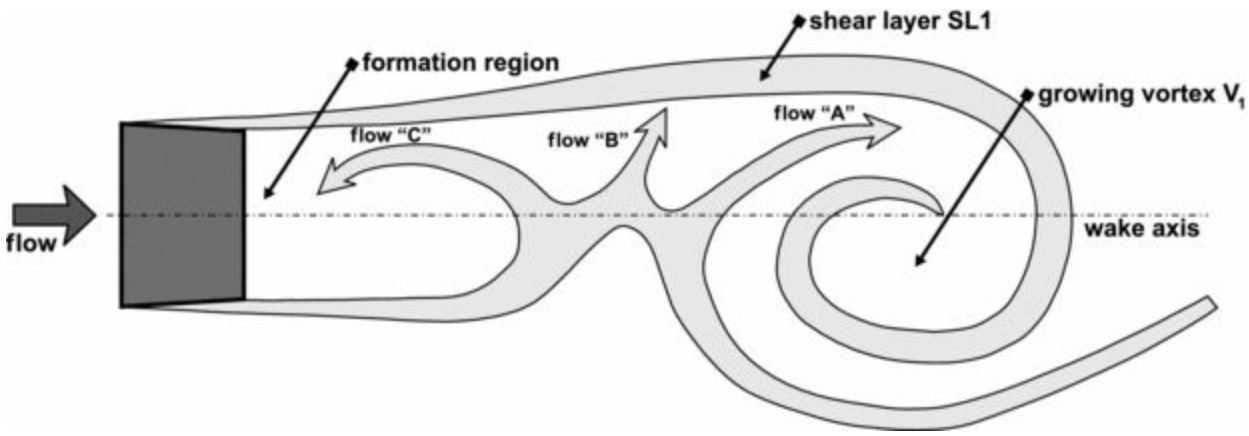

Figure 2: Vortices Shedding off of a Bluff Body (Bearman, n.d)

A vortex shedding from the bluff body exerts a force on the body. The vortices shed from alternating sides of the bluff body. During the oscillation cycle, one vortex is shed at the top and one at the bottom of the cycle. The shedding frequency can be matched with the natural frequency of a sprung mass system to create resonance. Matching the two frequencies would cause a significant translational movement of the bluff body as the spring force and vortex force line up. This motion can be used to excite a magnet-coil system, and to harvest wind energy as electricity. However, it is important to consider damping on this system. As energy is drained from the system due to drag, the amplitude of oscillation diminishes (Jus, 2014).

Airfoil Shape

The geometrical parameters for an airfoil can have a significant impact on the power efficiencies. In the 1920's and 1930's, the National Advisory Committee for Aeronautics (NACA) developed and thoroughly tested airfoils that were put into a cataloged system with specifications such as camber lines, maximum thickness, special nose features, etc. This information can be used to choose the proper airfoil for a specific application. There are several different asymmetrical airfoils that are commonly used on airplanes; however, for this application; we will be using a symmetrical airfoil so that there is the ability to extract energy from both directions.

The geometrical characteristics of an airfoil include a camber line, which defines the general shape of the airfoil. The chord is the line that joins the extremities of the camber line. The leading and trailing edges are the forward and rearward extremities. The angle created by the chord line in the camber line is θ (Bühler, 2018).

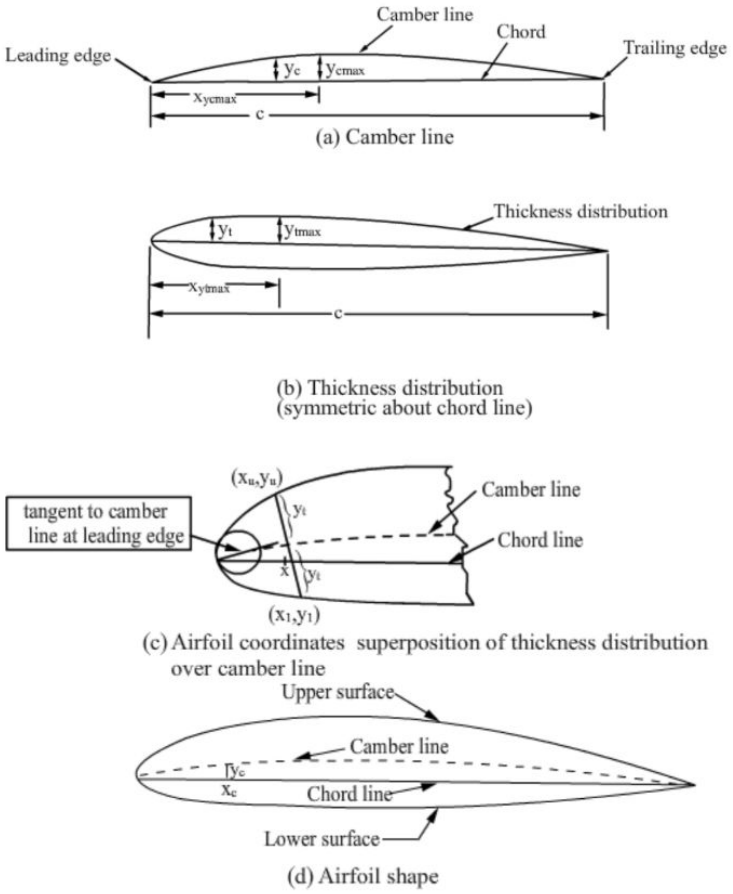

Figure 3: Airfoil Geometry (Bühler, 2018)

There are several different families of airfoils defined by NACA that vary in thickness and shape. The coordinates of the upper surface of the airfoil are defined by x_u and y_u and the lower surface by x_l and y_l in the following equations (Bühler, 2018):

$$x_u = x - y_t sin(\theta) \tag{2}$$

$$y_u = y_c - y_t cos(\theta) \quad (3)$$

$$x_l = x - y_t sin(\theta) \quad (4)$$

$$y_l = y_c - y_t cos(\theta) \quad (5)$$

The variables y_c and y_t are the coordinates at location x on the camber line. The thickness is defined by $tan\theta$ at location x. Another geometrical characteristic is the leading edge radius that is tangent to the camber line. The trailing edge also has the ability to have different geometrical characteristics that would affect the efficiency. The geometries described are shown in Figure 3 above.

A'fifah et. al conducted a numerical study on oscillating airfoils using three symmetrical NACA airfoils: NACA0012, NACA0015, and NACA0018 seen in Figure 4.

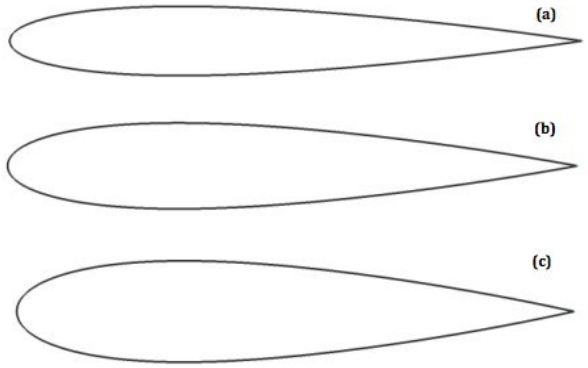

Figure 4: Airfoil Shapes (a) NACA 0012 (b) NACA 0015 (c) NACA 0018 (A'fifah et. al, 2016)

This study investigated the geometrical shape variations of trailing edge shapes, which included sharp, blunt, and round, along with thickness distribution and how it affected the power efficiencies. Specific fluid kinematic parameters were kept constant throughout the study including pitching amplitude, oscillation frequency, and heaving amplitude. The numerical study was conducted using ANSYS Fluent V.14.5 to observe the motion of the airfoil and used a 2D unsteady Navier-Stokes solver flow simulation to observe the performance behavior of flapping airfoils. In order to quantify the extracted power and efficiency, the time-averaged method was used. The instantaneous power was extracted from the sum of the heaving contribution and

pitching contribution. The power coefficient (C_P) is the ratio of the extracted power to the total available power.

The results of the study for a laminar flow and a Reynold's number of 1100 found that the thickness distribution affected the power efficiency by less than 2%. NACA 0015, with a sharp trailing edge, had the highest efficiency of 33.3% and NACA 0018 had the lowest efficiency of 31.4% for a non-dimensional frequency of 0.14. The peak efficiency value was at a frequency of 0.14 for each airfoil type. For higher efficiencies and the other trailing edge shapes, the efficiencies for a frequency of 0.16 ranged between 27.7% to 29.3% with a blunt trailing edge, with NACA 0015 being the lowest and NACA 0018 being the highest. For a frequency of 0.20, the efficiencies ranged from 22.2% to 24.2% for a round trailing edge, with NACA 0018 being the lowest and NACA 0015 being the highest. The results from this study are shown in Figure 5 below. From this, they were able to conclude that efficiency is generally unaffected by the thickness distribution at a low laminar flow.

Airfoil	Case 1		Case 2		Case 3	
	$f^* = 0.14$	Sharp edge	$f^* = 0.16$	Blunt edge	$f^* = 0.20$	Round edge
	$\bar{C}_P$	η	$\bar{C}_P$	η	$\bar{C}_P$	η
NACA0012	0.82	32.3%	0.72	28.4%	0.60	23.6%
NACA0015	0.85	33.3%	0.71	27.7%	0.62	24.2%
NACA0018	0.80	31.4%	0.75	29.3%	0.57	22.2%

Figure 5: Airfoil Thickness Effect for Different Trailing Edge Shapes when Re=1100 (A'fifah et. al, 2016)

The study also investigated a turbulent flow with a Reynolds number of $5x10^5$. The study found that NACA 0018 had the highest efficiency consistently throughout all trailing edge shapes and frequencies. The peak efficiency value was 44.5% with a non-dimensional frequency of 0.18. It was concluded that for turbulent flows, there is an increase in power efficiencies with a thicker airfoil.

Airfoil	Case 1		Case 2		Case 3	
	$f^* = 0.16$	Sharp edge	$f^* = 0.18$	Blunt edge	$f^* = 0.20$	Round edge
	$\bar{C}_P$	η	$\bar{C}_P$	η	$\bar{C}_P$	η
Naca0012	0.96	37.8%	0.82	32.1%	0.46	18.2%
Naca0015	1.03	40.3%	0.90	35.2%	0.73	28.5%
Naca0018	1.05	41.1%	0.99	38.9%	0.89	34.8%

Figure 6: Airfoil Thickness Effect for Different Trailing Edge Shapes when Re=5x10^5 (A'fifah et. al, 2016)

When comparing the effect of the trailing edge shape in a laminar flow, NACA 0015 was used at Reynolds number 1100. As seen in the graph below, the sharp edge had consistently higher power efficiencies than the round edge and blunt edge. The peak frequency is 0.14 for the sharp edge with an efficiency of 33.3% compared to the lowest edge shape, the blunt edge, which has about a 26.4% efficiency. When comparing the trailing edge shapes effect in a turbulent flow, NACA 0018 was used with the Reynolds number of 5x10^5. The peak power efficiency was at a frequency of 0.18 and the highest efficiency was the sharp trailing edge shape with an efficiency of 44.5%. From this, they were able to conclude that in a laminar and turbulent flow, a sharp edge shape will maximize the power efficiencies.

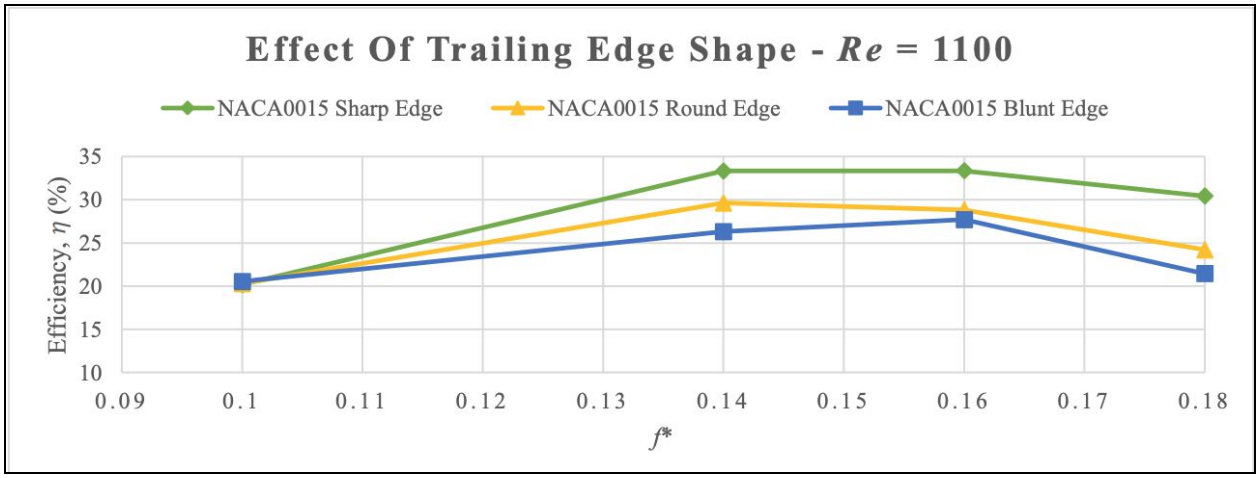

Figure 7: Effect of Trailing Edge Shape for NACA0015 Airfoil when Re=1100 (A'fifah et. al, 2016)

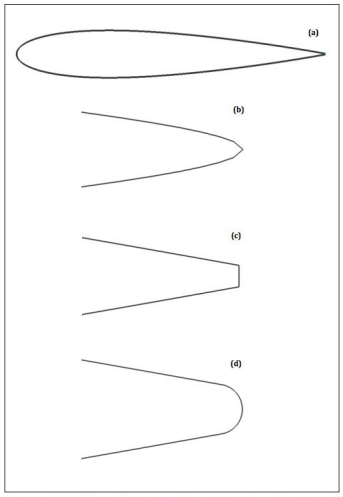

Figure 8: (a) Trailing Edge Shapes (NACA 0015) (b) close-up view of sharp edge (c) close-up view of blunt edge (d) close-up view of round edge (A'fifah et. al, 2016)

Important Parameters

Dynamic Stall

When designing aerodynamic bodies that are subject to oscillating or pitching motions, it is important to consider a phenomenon of dynamic stall. Dynamic stall is important when designing devices such as helicopters, flapping wings, and wind turbines because the violent vibrations and dangerously high loads can cause structure fatigue or failure (Corke, 2015). Dynamic stall occurs on airfoils when there are unsteady changes in the angle of attack. It is characterized by lift overshoot and massive flow separation. The dynamic stall vortex is what causes the different types of flow behavior.

The first step in dynamic stall is the formation of trailing edge vortices. Eventually, the separation point from these trailing edges moves towards the leading edge of the airfoil, which creates a shear layer. The instability of the flow is a Kelvin-Helmholtz instability, which occurs during the transition of different flows. Figure 9 below demonstrates Kelvin-Helmholtz instability.

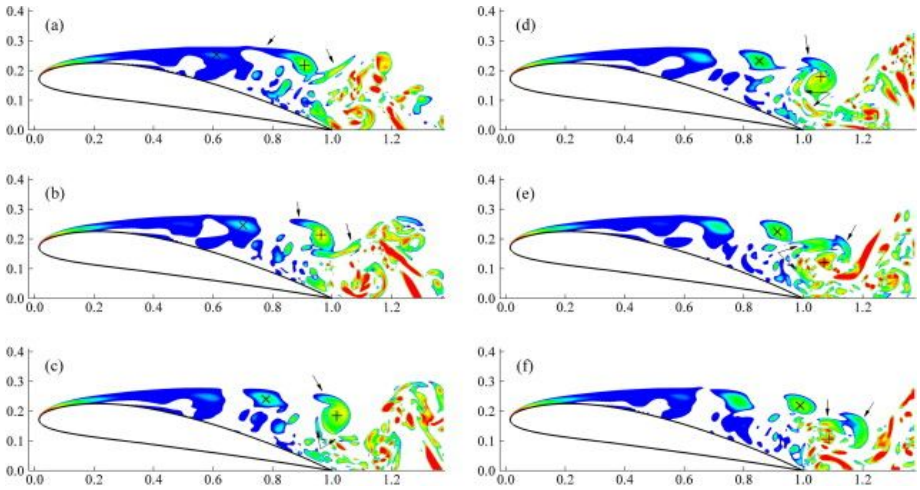

Figure 9: Kelvin-Helmholtz Instability on an Airfoil (Zhang, 2015)

The separation line eventually reaches the leading edge region which creates another shear layer. The Kelvin-Helmholtz instability rollers pair together causing a dynamic stall vortex (Corke, 2015). At this point, the trailing edge will dampen vortex shedding because it is at vorticity conservation. The dynamic stall vortex will eventually move downstream and cause a trailing edge vortex to form a shear layer that moves upwards. The trailing edge vortex shedding decreases the dynamic stall shedding. Dynamic stall is important when designing an energy harvester because it helps the airfoil to self-induce oscillations.

Oscillating Bluff Body

In order to predict the power output of the oscillating bluff body design in range of low wind velocities, a mathematical model similar to the one used for the airfoil design will be used. It is important to show the relationship between the dimensions of the bluff body, wind velocity, Reynold's number, Strouhal number, shedding frequency, amplitude, lift force, and spring constant. By adjusting these values, a prototype can be created that optimizes power output.

For bluff bodies, the Strouhal number has a tendency to range between 0.10 and 0.20. In order to find the shedding frequency of an ellipse, Equation 6 is used.

$$f_s = St\frac{U}{L_b} \tag{6}$$

$$L_b = \frac{4A}{P} \tag{7}$$

f_s : *shedding frequency of bluff body*

L_b : *characteristic length of bluff body*

U : *flow velocity*

St : *Strouhal number of bluff body*

A : *cross-sectional area of bluff body*

P : *perimeter of bluff body*

The natural frequency should be equal to the shedding frequency. We can set the natural frequency equal to the shedding frequency in Equation 8 to solve for the k value as long as a mass is defined.

$$\omega_n = \sqrt{\frac{k_{eq}}{m}} \tag{8}$$

ω_n : *natural frequency*

k_{eq} : *equivalent spring constant*

m : *mass of the system*

This equivalent k value accounts for the total value of all the springs in a given system. When the bluff body is suspended at rest, there is an equal extension of all springs allowing the forces acting on the bluff body to be calculated. From this, we can solve for desired spring constants.

Fluttering Airfoil

Flutter is a phenomenon that occurs when aerodynamic forces excite a mass. It is caused by two structural modes, pitch and plunge. The pitch mode is rotational whereas the plunge mode is a linear up and down motion. Aeroelastic flutter is a dynamic instability of an elastic structure in a fluid flow and the force that is exerted by this flow causes the body to deflect which causes a vibration. The plunging and pitching equations can be represented by the following equations.

$$Plunging:\ h(t) = h_o cos(2\pi f t + \phi) \tag{9}$$

$$Pitching:\ a(t) = \alpha_o cos(2\pi f t) \tag{10}$$

h_o : *pitch amplitude*

Φ : *phase difference between pitching and plunging motion*

a_o : *angle of attack*

f : *frequency*

t : *time*

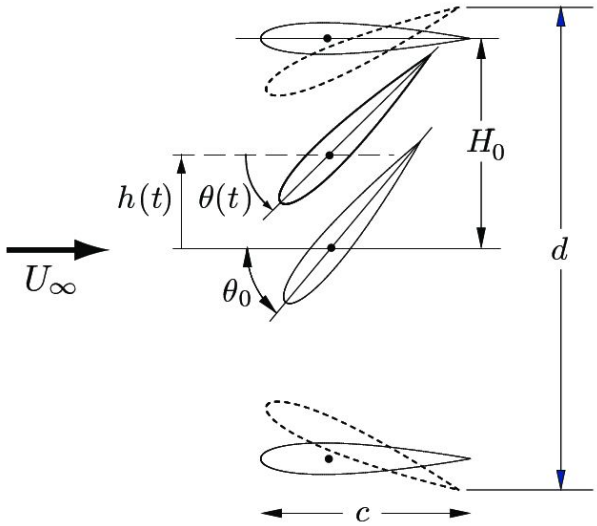

Figure 10: Pitching and Heaving Motions of an Airfoil (A'fifah et. al, 2016)

Two relevant types of mechanical vibrations are free vibrations and forced vibrations (A'fifah et. al, 2016). Free vibrations are when the body is given an initial displacement and is a result of potential or kinetic energy within in the system. Forced vibrations are when there is a periodic external force that causes the airfoil to vibrate. In the systems designed in this project, forced vibrations will occur. These designs will take advantage of the vortex shedding and aeroelastic flutter to cause the airfoil and bluff body to oscillate. Similarly to the bluff body, shedding frequency and resonant frequency are set equal, but this time it is solved in the opposite direction.

For this design, lift force is calculated first using Equation 11.

$$F_L = \tfrac{1}{2} C_L \rho A_a V^2 \tag{11}$$

F_L : *lift force of airfoil*

C_L : *lift coefficient of airfoil*

ρ : *density of air*

A_a : *cross-sectional area of airfoil*

V : velocity of fluid flow

The different airfoil shapes have been studied by the Computational Engineering Design Group, out of University of Southampton, UK and respective lift coefficients have been proven under a range of angles of attack. Finding the maximum lift force, we can solve for the individual spring constants using Equation 11. When the force is at a maximum, the airfoil, in theory, should be fully extended in one direction. Using this method, our fluttering airfoil was designed.

Energy Harvesting

The motion of the bluff body and airfoil designs due to wind provides renewable energy that can be converted into electricity. Our designs turn wind energy into kinetic energy of the moving bodies. In order to harvest kinetic energy into electricity, a transducer is required. For mechanisms that use ambient vibrations to harvest wind energy as an alternative to batteries, transduction methods such as, electrostatic, electromagnetic and piezoelectric are often used.

Electrostatic

Electrostatic energy harvesters involve comb finger electrodes or parallel-plate electrodes as variable capacitors that are biased with external voltage sources and varied as a function of ambient vibrations (Yang, 2010). Charged plates or fingers are separated by the work done by mechanical vibrations against the electrostatic attractions, which generates a charge (Elliott, 2012). These systems are connected to circuits that collect electricity as the change in capacitance occurs (Diltz, Gagnon, O'Connor, & Wedell, 2017). The change in capacitance can either cause a voltage increase in a constant charge system, or inversely a charge increase in a constant voltage system (Abdulmunam, Taha, & Ivey, 2012). By fixing either the voltage or charge with a varying capacitor, the non-fixed variable must adjust to fit Equation 12.

$$Q = CV \tag{12}$$

Q : *charge*

C : *capacitance*

V : *voltage*

Energy generated in each cycle can be solved using Equation 13.

$$E = \frac{1}{2}Q^2\left(\frac{1}{C_{Min}} - \frac{1}{C_{Max}}\right) \tag{13}$$

This method is not passive, meaning that a small voltage is necessary for the system to induce a variance in capacitance, which will produce an increased voltage output. For small-scale wind energy applications this may be a huge disadvantage for efficiency. At a larger scale, a small input voltage may be negligible. In a study conducted in 2012, electrostatic energy harvesting was investigated as an option for a new macro scale wind turbine replacing electromagnetic generation (Abdulmunam, Taha, & Ivey, 2012). The electrostatic model was found to have a better efficiency than electromagnetic because electrostatic produces direct current voltage while electromagnetic required a conversion to DC voltage. The higher efficiency in a generator causes a deduction in cost of a generation system. The concept is described in Figure 11 below.

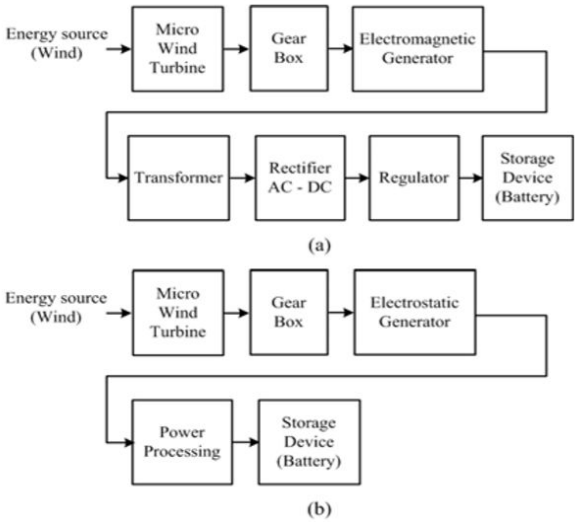

Figure 11: Tracking the flow of energy through EM and ES harvesting systems (a) Electromagnetic (b) Electrostatic (Abdulmunam, Taha, & Ivey, 2012)

Another issue with this technology is that it requires mechanical stoppers to prevent short-circuiting which results in increased mechanical damping (Khan, 2016). Although, electrostatic has advantages over piezoelectric materials at low accelerations (10^{-2} m/s) and inversely at high accelerations (10^{2} m/s) as well. At low accelerations, electrostatic experience lower energy losses than piezoelectric material and at higher accelerations the dielectric breakdown limit in piezoelectric material limit its ability to harvest energy (Elliott, 2012). Figure 12 below gives a comparison of piezoelectric and electrostatic effectiveness at a range of accelerations from 10^{-2} m/s^2 to 10^{2} m/s^2. System Effectiveness can be measured by a system's ability to achieve its requirements with respect to availability, dependability and capability.

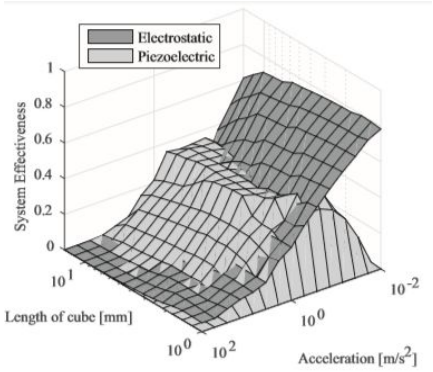

Figure 12: Comparison of power output and system effectiveness between electrostatic and piezoelectric material for Microelectromechanical systems (MEMS) (Elliott, 2012)

Piezoelectric

Piezoelectric technology uses mechanical strain of a piezoelectric material under loaded force (Yang, 2010). When stress is applied to the material the direction of polarization changes that produces an electric field (Ledoux, 2011). The output voltage has a proportional correlation to the stress of the material. There are two equations used to find the output voltage. Equation 14 finds electric field strength by dividing the density displacement by the permittivity of the material.

$$E = \frac{D}{\varepsilon} \tag{14}$$

E : electric field

D : density displacement

ε : permittivity of the material

Equation 15 uses Hooke's Law for linear elastic materials where stress is calculated by multiplying elastic modulus by the strain.

$$\sigma = E\varepsilon \tag{15}$$

σ : stress

E : elastic modulus

ε : strain

These equations are combined with the matrix of electric permittivity to solve for the piezoelectric effect (Abdulmunam, Taha, & Ivey, 2012).

Experiments using piezoelectric material to harvest vibrations have discovered that an increase in wind speed does not correlate with an increased output voltage (Zhang, 2017). It has been found that the impact frequency is an important variable. With Piezoelectric technology, there is no input voltage source required like electrostatic (Elliott, 2012.). The efficiency of a typical piezoelectric material ranges from 30% to 75%. Both piezoelectric and electrostatic are ideal for MEMS; however, electromagnetic is better suited for larger power requirements.

Electromagnetic

Electromagnetic energy harvesting is used more to produce large power output, but in recent years it has been found that electromagnetic systems the size of several tens of millimeters can provide a few hundred microwatts (Yang, 2010). An advantage of using electromagnetic power generation is that it does not require an initial voltage like electrostatic systems. Electromagnetic energy harvesters use a permanent magnet that moves across or through a coil to generate a changing magnetic flux. Magnetic flux is defined by the equation below.

$$\phi = BA \tag{16}$$

ϕ *: magnetic flux*

B : magnetic field

A : area perpendicular to magnetic field

By multiplying the field strength of the coil material by the area, we can calculate magnetic flux. The change of flux over time induced by the vibration of a magnet is how the technology generated voltage. The amount of output voltage is solved using the equation below.

$$\varepsilon = -N\frac{d\phi}{dt} \tag{17}$$

N : number of turns in coil

t : time

The efficiency of the system depends on how many flux lines are cut by the coil and the distance of the magnet from the coil.

Decision Matrix

In order to decide which technology is most appropriate, a weighted decision matrix was created. The most important criteria to a small-scale wind energy device were listed in the first column including efficiency, cost, durability, input voltage requirement, simplicity of design, and power output. Each criterion was weighted by the level of importance on a scale of 1 to 6, with 6 being the most important. Under each type of energy harvesting technology a number was assigned from 1 to 10, where low values indicate the characteristic of that technology show negative effects on said device and inversely with high values. Weights are then multiplied by each technology's values per criterion and summed to one value. After values were calculated, it was found that the electromagnetic technology had the highest score therefore the best fit for small-scale wind energy.

Table 1:
Transducer Decision Matrix

For Small Scale Wind Energy Devices	Weight	Electromagnetic		Piezoelectric		Electrostatic	
Efficiency	2	6	12	4	8	5	10
Cost	3	7	21	9	27	7	21
Durability	1	8	8	10	10	8	8
Input Voltage Requirement	4	10	40	10	40	1	4
Simplicity of Design	5	7	35	8	40	5	25
Power Output	6	10	60	8	48	6	36
			176		173		104

Past Research

Inspirations of our project come from research on vortex-induced vibrations and transverse galloping from past WPI major qualifying projects (MQP) and research conducted by Cornell University and Zephyr Energy. Combining these wind-motion concepts allowed us to improve and build upon previous studies.

Cardboard Cylinder Energy Harvester MQP

This project researched and designed a wind energy-harvesting device using vortex shedding. The prototype consisted of a cardboard cylinder attached to four springs oscillating in a vertical motion. The transducer was electromagnetic with a simple magnet and coil assembly. Our project will build off of this project in a few ways. One of the aims of our project is to change and optimize the bluff body shape, also looking towards another degree of freedom, in the form of a hinged airfoil. We also optimized the transducer mechanism to get a better efficiency and power output from our device.

Piezoelectric Tree Concept

A study on vortex-induced vibrations was conducted at Cornell University. The goal was to create a wind energy device that imitated tree branches swaying in the wind. This project made use of a piezoelectric transducer to convert the mechanical vibrations in electricity. These piezoelectric properties were found in the polyvinylidene difluoride (PVDF) “stems” connected to the bluff bodies. Each bluff body would create vortex shedding in wind, and this would move the piezoelectric stems and generate electrical energy. The results of the piezo-tree were 100 pW of electricity. This small power output was caused by the weak piezoelectric strain coefficient of

PVDF. The study then added “leaves” made of plastic and connected them to the “stems” to flutter. They found that power increased by 100 times with the leaves, and tried other various positions of shapes, resulting in different amounts of power output. The study did not provide all values of power output; however, the highest output was a result of vertical “stems” and horizontal “leaves.” Overall, this study was successful in optimizing a low-cost, piezoelectric wind-harvesting device that mimics a tree.

Zephyr Windbeam

The Zephyr Windbeam is a small-scale alternative energy device that takes advantage of wind speeds as low as 2 mph to harvest energy. This oscillating beam is a half cylinder to induce transverse galloping. AC power is generated using an electromagnetic induction system which captures energy on the downward cycle of the beam oscillation. Because of the low output, more testing has been conducted on a smaller scale, which could be useful in many applications such as HVAC sensors, military, weather stations broadcast towers, emergency lights, and recharging personal electronics. Although there is not a standard product, the opportunities the technology has are infinite.

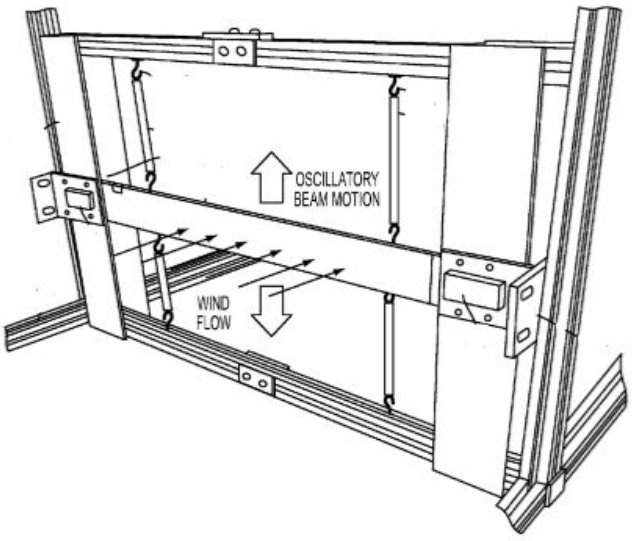

Figure 13: Wind Beam Energy Harvesting Device (Throp, 2015)

Studies by Zephyr have shown how scalability of the beam length and the velocity of fluid flow both increase the power output of the device. Figure 14 below shows the power output from testing three different sizes of the wind beam. Ranging from 5 inches to 30 inches, the Windbeam generated a power output of 0 to 3 watts (Wright, 2016).

Beam Length	30″	18″	5″
Power Output	0 - 3 W	0 - 40 mW	0 - 6 mW

Figure 14: Beam length effects on power output (Wright, 2016)

Additionally, a controlled study was performed to show the effects of increasing wind speed on the power output. As the wind speed increased from 6 mph to 9 mph, the power output increased from 1.62 mW to 5.94mW as seen in Figure 15 (Wright, 2016).

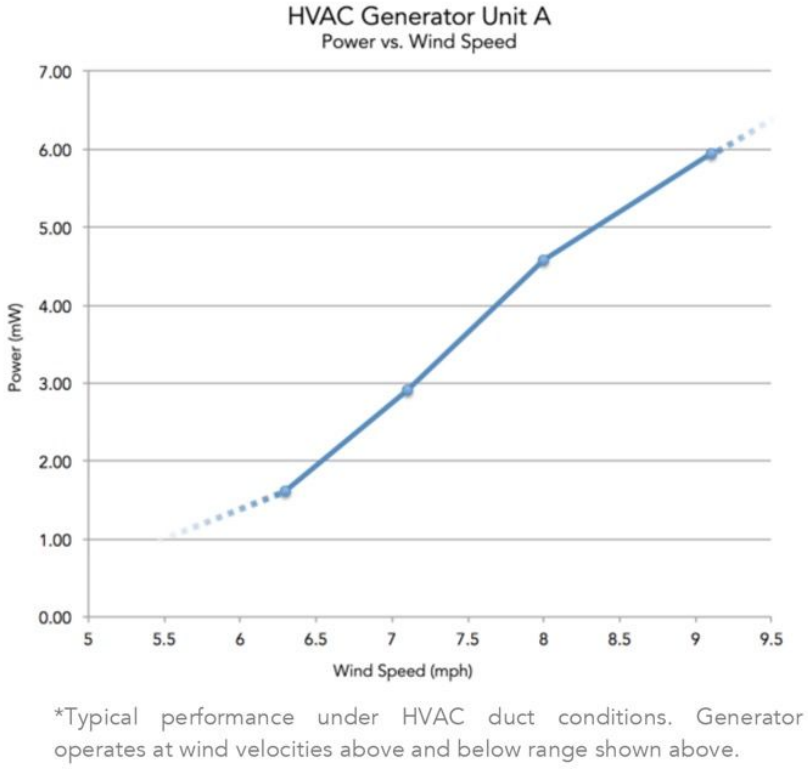

Figure 15: Wind Speed Effect on Power Output (Wright, 2016).

Using research and past projects, this study was developed to prove the ability to harvest electricity using natural phenomenon. Through the design process, calculations were made to develop an effective design for an oscillating bluff body along with a fluttering airfoil.

Benefits of Small-Scale Energy Harvester

Small-scale wind energy is a growing field that is becoming higher in demand and needs more engineers and scientists to investigate the potential that wind energy can bring to small applications. It is a portable way to encourage the use of renewable energy and allows for easy deployment of these products due to their reduced interfacing costs. These small-scale energy harvesters can be used for several off-grid sensors or other small-scale applications around a home or building at any height and in any location at low wind speeds. This can be beneficial for sensors that are battery powered and require replacements several times per year. This would help to prevent the cost of replacing batteries and the waste produced by the batteries. Examples of these applications could be HVAC sensors or actuators, sensor for seismic monitoring, electrification in a rural area, or electrification emergency preparedness and disaster relief. Due to its adaptability, the designs can also be scaled or put into series with several of the same harvesters to make the power output even greater.

Small-scale wind helps to reduce the amount of environmental impacts. The design has minimal noise pollution and does not have a large impact on the environment like larger scale wind energy harvesters. In comparison, larger wind turbines produce a significant amount of noise pollution ranging from 40-105 decibels depending on the distance from the turbine. Larger wind turbines also can have an effect on the wildlife that comes into contact with the device. On average, 148,000 to 328,000 birds die each year from wind turbines; however, one of the larger issues in the wind industry is the amount of bats that die from wind turbines (Eveleth, 2013). There are 600,000 to 900,000 bats that are killed by wind turbines every year in the U.S. (Curry, 2015). The current solution to combating bat and bird fatalities is curtailment, which reduces the

amount of energy produced. The small-scale wind energy harvester is beneficial because it will not affect species like bats and birds the way that wind turbines move due to their reduced size. This also allows for easy transportation and can remain in an environment without drastically affecting the surrounding ecosystem.

Energy Harvester Designs

Bluff Body

The bluff body design was inspired by the Zephyr Windbeam. It was designed to be approximately 50g and less than 2 cubic feet in order to be within the constraints of the wind tunnel. Its cross section had the shape of an ellipse, and the two furthest sides of the beam each had two hooks to allow two sets of springs to be attached. The suspended bluff body was connected to hooks on the side supports that were made to be symmetrical to ensure that the airflow remained the same throughout the system. The main design aspect that we focused on was the distance between the side supports, rather than the shape. Adjustments were made to the height of the side supports to allow the bluff body to oscillate a greater distance without damping. The final assembly of the bluff body harvester is pictured below, without the 4 springs suspending the body.

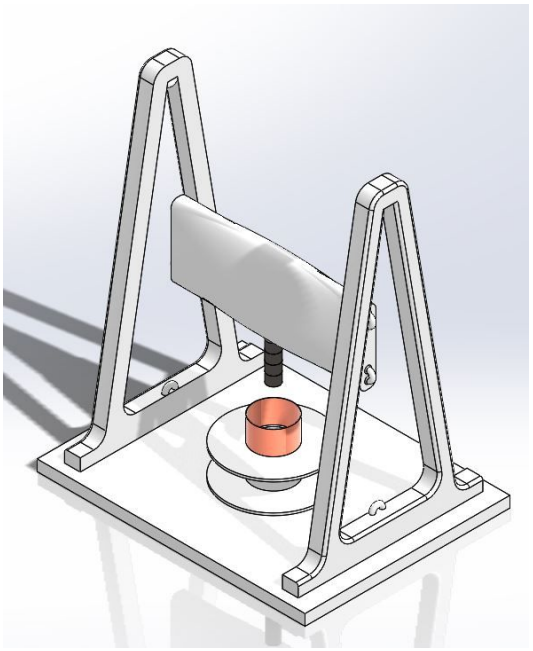

Figure 16: Bluff Body Harvester Design

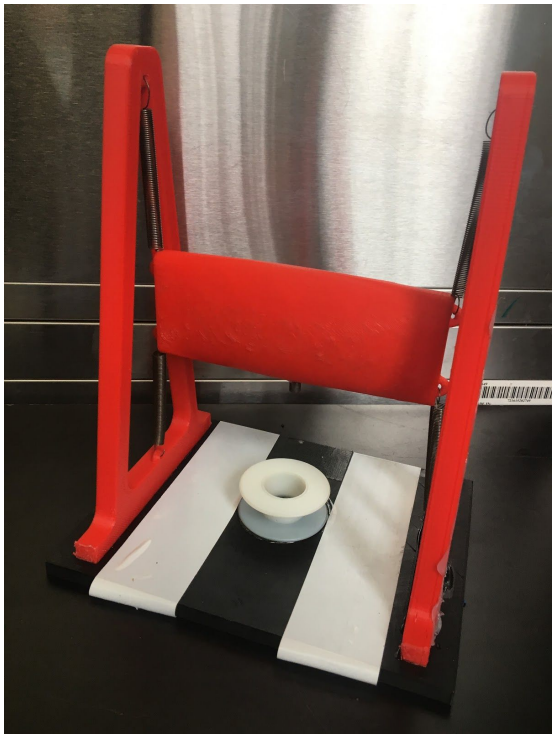

Figure 17: Bluff Body Harvester Prototype

Airfoil

The airfoil energy harvester prototype was designed to allow for a full cycle of motion horizontally. A larger base was needed compared to the bluff body design, but the surface area restrictions of the 3D printers prohibited printing the base as one part. Therefore, the base was printed as two parts, and a laser cut piece of plywood secured the two prints together. The purpose of increasing the width of the base was to allow the airfoil to displace a further distance along the tracks, so the airfoil would have the freedom it needed to flutter properly.

The slider design used a nylon "U" shaped rod on the bottom and two nylon dowels on the top to allow for ease of motion. The four springs were attached to the sides of the sliders that had eye bolts, and to the hooks on the sides. The final airfoil harvester design is demonstrated in Figure 18 below.

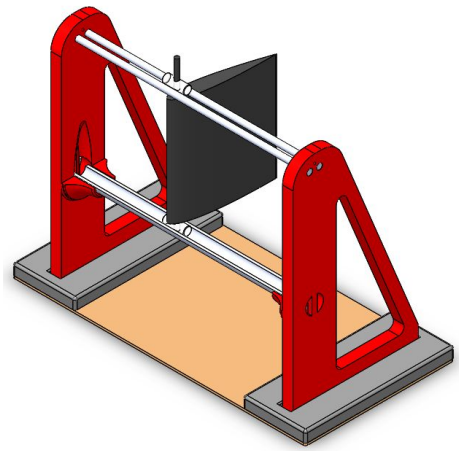

Figure 18: Airfoil Design

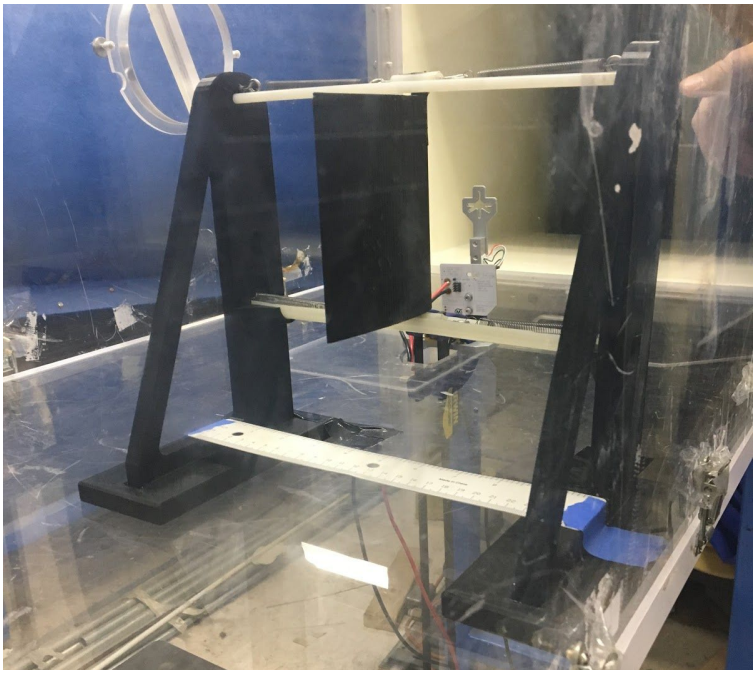

Figure 19: Airfoil Harvester Prototype

Design Calculations

This section focuses on the theoretical calculations that determined specific parameters necessary for our designs and predicted the output voltage of the bluff body energy harvester and the airfoil energy harvester. The values for each variable were determined from previous research or by the designers.

Bluff Body Design

In order to find the Reynolds number, the maximum flow speed and the kinematic viscosity of air was needed. The average flow speed of wind was estimated to be about 5 m/s after observing the wind speeds in Worcester, MA.

$$Re = \frac{UL_b}{\nu} = 1.39 * 10^4 \quad (18)$$

$$\textit{bluff body characteristic length} = L_b = 0.039\ m$$
$$\textit{kinematic viscosity of air} = \nu = 1.48 * 10^{-5}\ m^2/s$$
$$\textit{maximum flow speed} = U = 5.0\ m/s$$

After determining the Reynold's number, the mass ratio was calculated. The mass of the bluff body was required as well as the displaced fluid mass. The displaced fluid mass was found by multiplying the bluff body volume by the air density. The volume of the bluff body was estimated during the design process when the cross-sectional shape was determined.

$$\textit{air density} = \rho_{air} = 1.23\ kg/m^3$$
$$\textit{volume of bluff body} = V_{bluff\ body} = 1.85 * 10^{-4}\ m^3$$
$$\textit{mass of bluff body} = m_{bluff\ body} = 0.05\ kg$$

$$m_{displacement} = \rho_{air} * V_{bluff\ body} = 2.26 * 10^{-5}\ kg \tag{19}$$
$$m^* = \frac{m_{bluff\ body}}{m_{displacement}} = 229 \tag{20}$$

$$m_{displacement} : \textit{displaced mass}$$
$$m^* : \textit{mass ratio}$$

Using the mass ratio, the low reduced mass-damping product was calculated. This parameter is important because if the mass-damping is closer to zero, the system is closer to an undamped system, which allows for continuous or increased oscillation.

$$\zeta(m^* + 1) < 0.05 \tag{21}$$
$$m^* = 229$$
$$\zeta < 2.2 * 10^{-4}$$

The Strouhal number was determined to help find the shedding frequency of the oscillating bluff body by using the characteristic length of the bluff body, Reynolds number, and maximum flow speed.

$$Re = 1.39 * 10^4$$

$$St = 0.198 * (1 - \frac{19.7}{Re}) = 0.2 \quad (22)$$

The frequency of vortex shedding was determined after finding the Strouhal number for the design. The theoretical shedding frequency should be equal to the natural frequency.

$$\omega_n = f_s = St\frac{U}{L_b} = 25.6\ Hz \quad (23)$$

Next, we used the natural frequency to calculate an equivalent k value for the sprung mass system. Using the equivalent k value for the system, we solved for our desired spring constants.

$$\omega_n = \frac{1}{2\pi} * \sqrt{\frac{k_{eq}}{m_{\ bluff\ body}}} = 25.6\ Hz \quad (24)$$

$$m_{bluff\ body} = 0.05\ kg$$

$$k_{eq} = 1294\ N/m$$

There is an equal extension of all four springs when the bluff body is suspended at rest. The free body diagram below shows the applied forces from the springs acting on the bluff body.

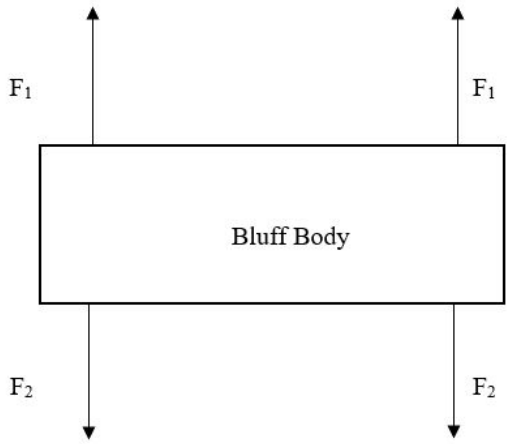

Figure 20: Bluff Body Free Body Diagram

The equations below give us the forces exerted by the springs, where F_1 acts up, and F_2 acts down.

$$F_1 = k(x_f - x_o) \quad (25)$$

$$F_2 = -k(x_f - x_o) \quad (26)$$

x_f *: stretched spring length*

x_o *: spring length in equilibrium*

Equations 25 and 26 give the equilibrium state of the system, where all springs are stretched to their initial amount. At this state both forces are equal and opposite. The sum of F_1 and F_2 is the total force F_T exerted by the spring system on the bluff body. Equation 27 below shows the total force on the mass when it is displaced a distance of *x* in the negative direction.

$$F_T = F_1 + F_2 \quad (27)$$

$$F_T = k((x_o + x) - x_o) - k((x_o - x) - x_o) \quad (28)$$

$$F_T = 2kx \quad (29)$$

F_T *: sum of spring forces*

x : spring displacement

In the positive direction, the total force is $2kx$. This is a centering force; if x is in the positive direction, the force will be in the negative direction. This results in an equivalent k for the 2-spring system of $2k$. There are two of these systems acting in parallel, as seen in the free body diagram above, so the equivalent k value is doubled to $4kx$ for the natural frequency calculations. Next, we can calculate the spring constant by dividing the force of all springs into four equal parts.

$$k_{eq} = 4kx \tag{30}$$

$$k = 323 \text{ N/m}$$

This theoretical value would determine the maximum spring constant since it was calculated using the maximum mass of the bluff body and maximum wind speed. We determined a range of smaller k values to use for our design, assuming that the mass of the bluff body and wind speeds would be less. We tested four springs with spring constants ranging from 10.5 to 77.1 N/m, because we wanted our prototypes to work in low wind areas. After manufacturing the bluff body, we determined the actual weights and dimensions of the part as the SolidWorks model did not accurately represent the actual measurements of the bluff body. The bluff body was remeasured to be 0.037 kg. We were then able to calculate the theoretical natural frequency of the bluff body design using the same equations above. After determining the natural and shedding frequencies, we were then able to find the theoretical wind speed that would help us find the resonant frequency wind speed in the wind tunnel during our testing procedure. The theoretical calculations can be found in Table 2 below.

Table 2:
Theoretical Calculations using Actual Bluff Body Dimensions

Spring Type	**A**	**B**	**C**	**D**
Spring Constant (N/m)	10.5	15.8	38.8	77.1
Theoretical Natural Frequency (Hz)	5.4	6.6	10.3	14.5
Theoretical Shedding Frequency (Hz)	5.4	6.6	10.3	14.5
Theoretical Wind Speed (m/s)	1.0	1.3	2.0	2.8

Airfoil Design

The value for the cross sectional area of the airfoil is determined based on the cross-sectional area normal to the lift force. This is found from our airfoil design using a NACA 0015 airfoil. The cross-sectional area is 0.01 m^2. The size of the airfoil was chosen based on the ratio of the size of the airfoil to the size of the structure. The structural design size was chosen based on the dimensional specifications of the wind tunnel used for testing.

$$A = cross-sectional\ area\ normal\ to\ lift\ force\ =\ 0.01\ m^2$$

The lift coefficient was determined through our research of a NACA 0015 airfoil. The research was conducted in a controlled wind tunnel at the University of Gazi, Faculty of Technology (Şahin, 2015). The airfoil was forced to be stationary. This research as seen in the graph below, shows that at the maximum angle of attack, 45 degrees, the lift coefficient was approximately 1.05. At this angle of attack the assumption is made that this is the point with the maximum lift force.

$$\theta\ =\ Angle\ of\ attack\ =\ 45^o$$
$$C_L\ =\ lift\ coefficient\ = 1.05$$

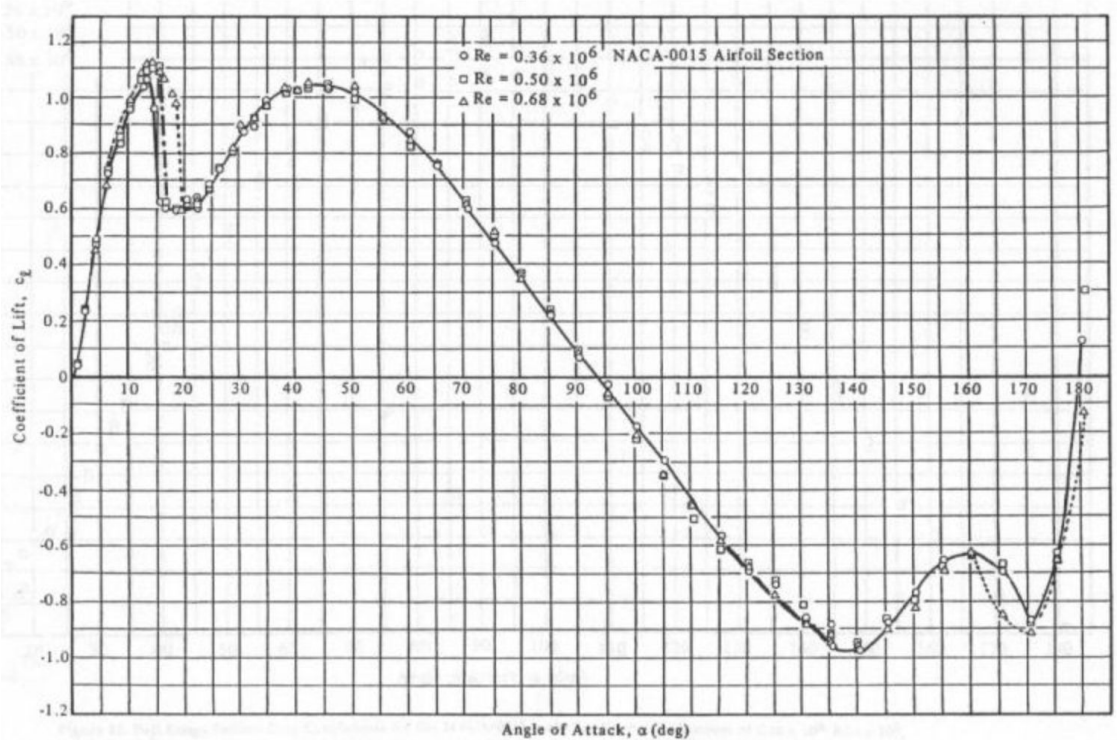

Figure 21: Lift Coefficient from 0-180 Angle of Attack for NACA 0015 Airfoil (Sheldahl, 1981)

Using the average wind speed in Worcester, MA, we are able to estimate the maximum lift force on the airfoil at the highest angle of attack.

$$v = 5.0\ m/s$$
$$\rho = 1.225\ kg/m^3$$
$$F_L = \tfrac{1}{2} * C_L * \rho * A_a * v^2 = 0.1608\ N \tag{31}$$

If we assume the unstretched spring is approximately 0.0762 m (3 in) and the stretched spring is assumed to be 0.1905 m (7.5 in), the spring constant is calculated by finding the displacement of the springs and the spring constant.

$$0.1608\ N = 2 * k * (0.1905m - 0.0762m)$$
$$k = 0.7034\ \text{N/m}$$

From this, we can calculate the theoretical natural frequency of the airfoil. If the mass of the airfoil is about 0.05 kg and the spring constant is 0.7034 N/m, the natural frequency is calculated to be 1.2 Hz.

$$\omega = \sqrt{\frac{4k}{m}} \tag{32}$$

$$\omega = \sqrt{\frac{4(0.7034)}{0.05}} = 7.5\ rad/s = 1.2\ Hz$$

In order to have the airfoil oscillate, the natural frequency and shedding frequency should be equivalent. The Strouhal number was necessary to find the shedding frequency. The Strouhal number was found through our research and at a maximum angle of attack of 45 degrees, it is estimated to be approximately 0.18. The wind velocity was also taken from the average wind speed in Worcester, MA. The chord length was determined by using the NACA 0015 airfoil and designing the airfoil to be proportioned large enough to have the ability to oscillate in the wind, but also small enough that the airfoil weight was as small as possible. Using the equations for the NACA 0015 airfoil (Equations 2, 3, 4, and 5), the chord length was measured to be 0.12 m. The shedding frequency is calculated to be 7.5 Hz.

St_a = *strouhal number* = 0.18
U = *wind velocity* = 5 m/s
L_a = *chord length* = 0.12 m

$$f_s = \frac{St_a * U}{L_a} = 7.5 \text{ Hz} \tag{33}$$

The feasibility in creating a system with spring constants as low as 0.7034 N/m to induce aeroelastic fluttering was not reasonable. In order to use stronger springs in the airfoil wind energy harvester, the lift force had to increase which could be adjusted by increasing the wind velocity.

Methodology

Our main goal was to design and build proof of concept prototypes. We created two small-scale wind energy prototypes that generate power using electromagnetic transducers. The purpose of this project was to investigate the differences in power output from a vertically oscillating bluff body and a horizontally-oscillating airfoil with the same electromagnetic transducer. These devices demonstrate how wind can be harvested through vortex-induced vibrations. Through controlled wind velocity tests, we analyzed how both prototypes perform in various conditions and compare results based on the total amount of power generated. We achieved these goals through the following objectives:

1. Design and construct prototypes with an oscillating bluff body and an airfoil.
2. Conduct a test with controlled wind velocities to determine the electrical output of each design.
3. Design and construct an electromagnetic transducer for the airfoil and bluff body design.

Objective 1: Design and construct prototypes with an oscillating bluff body and an airfoil.

Energy Harvester Design

The energy harvester design consisted of similar structures for both the bluff body and airfoil designs. Based on our calculations from our design process section, we were able to determine the parameters for our designs. The outer dimensions of the structure had to be small enough to fit in the wind tunnel testing area, therefore the dimensions of the prototype remained within the constraints of 2 ft x 2 ft. The outer structure consisted of a base and two sides made out of PLA. The bluff body sides had one hook at both the top and bottom of the sides to hold the springs. These bluff body sides were connected to a large rectangular base. In the airfoil design, the sides were connected to two stationary nylon tracks that each held a nylon slider connected to the top and bottom of the airfoil. These nylon sliders were connected to the sides with springs and eye bolts. The bill of materials for each design is in Table 3 and Table 4. Both designs include the same coil, magnet, and springs.

Table 3:
Bluff Body Design Bill of Materials

PART NAME	QTY	MTL	MANUFACTURING	DIMS
Base	1	PLA	3D Print	Length: 215 mm Width: 165 mm
Side	2	PLA	3D Print	Height: 250 mm Width: 15 mm
Coil	1	Copper	Purchase	Height: 20 mm ID: 25 mm
Magnet	1	Neodymium	Purchase	11,000 - 12,300 Gauss with varying sizes
Bluff Body	1	PLA	3D Print	15mm x 58.42mm x 152.4mm
Spring	4	Spring steel	Purchase	10.51-77.06 N/m

Table 4:
Airfoil Design Bill of Materials

PART NAME	QTY	MTL	MANUFACTURING	DIMS
Base	1	PLA	3D Print	Length: 305 mm Width: 165 mm
Side	2	PLA	3D Print	Height: 255 mm Width: 150 mm Slider Hole Diameter: 20 mm Distance of Holes: 155 mm
Coil	1	Copper	Purchase	Height: 20 mm ID: 25 mm
Magnet	1	Neodymium	Purchase	11,000 - 12,300 Gauss with varying sizes
Airfoil	1	PLA	3D Print/Cut	Chord Length: Length chord: 110 mm Height: 110 mm Axle Diameter: 5 mm Axle Height: 10 mm
Spring	4	Spring steel	Purchase	10.51-77.06 N/m
Track	2	Nylon tube	Purchase	ID: 12.7 mm OD: 19.05 mm Length: 254 mm
Slider	2	Nylon rod	Purchase	OD: 4.7625 mm Length: 20 mm
Steel Eyebolts	4	Stainless Steel	Purchase	Eyehook Diam: 3/16” Length: ¾” Thread Length: 5/16”

Bluff Body & Airfoil Design

The bluff body design was made of PLA with four 3D printed hooks to hold the suspension springs. The suspension springs were attached to the hooks on the outer structure. Attached to the bottom of the bluff body with adhesive were 4 neodymium magnets each with a diameter of 4 mm, height of 2 mm, magnetic strength of 12,300 Gauss and weight of 1 g. A coil was vertically mounted on the base directly below the magnets. This coil was made up of a copper wire with a thickness of 0.1 mm and approximately 50 turns. When the bluff body oscillated, the magnet was inserted in and out of the coil to produce a voltage.

The airfoil was also made of PLA and had a chord length of 110 mm, height of 110 mm, and largest diameter of 12 mm. The airfoil had an axle with a diameter of 0.15 mm placed ⅓ of the distance from its leading edge. The axle moved along the slider on a track connected to the outer structure. The slider was connected to the springs that were connected to the outer structure.

Objective 2: Conduct a test with controlled wind velocities to determine the electrical output of each design.

Controlled Bluff Body and Airfoil Wind Tunnel Experiment

For this study, we tested the motion of the bluff body and airfoil. The goal of this study was to determine the speed at which each spring constant achieved resonant frequency. With this data, we determined the maximum energy output. During this stage of testing, the wind speed varied using the controlled environment of a wind tunnel. There were 4 different spring types with k-values ranging from 10.5 N/m to 77.1 N/m. Each spring type was tested at its calculated wind velocity based off of its resonant frequency.

During each experiment for the bluff body energy harvester, displacement from resting state was measured along with frequency of each oscillation cycle. Using a ruler and video camera, observations were made to determine the peak displacements of the bluff body along with the time it took for a full cycle to be completed. The data from testing gave us a correlation of spring constant and wind velocity.

For the airfoil energy harvester, we wanted to find similar variables determined in the bluff body testing process. By finding the resonant frequency, we could better determine the theoretical power output. This was determined by finding the resonant frequency of 4 different springs attached to the airfoil with the same k-value ranges of 10.5 N/m to 77.1 N/m.

During this experiment, displacement from the resting state was measured to find the translational displacement of the airfoil. We determined displacement by measuring the difference in location from the resting state of the dowel with the maximum extension reached in one cycle.

After determining the optimal springs to produce a maximum voltage output for each design, we tested the bluff body in the wind tunnel again with the magnets attached to the bluff body and a coil attached on the base. We conducted the same wind test while connecting the coil to a multimeter to determine maximum voltage output. After we determined the electromagnetic

transducer specifications for the bluff body energy harvester, we tested the transducer to convert the energy into an electrical current. The airfoil energy harvester would have undergone the same wind test with an attached magnet and coil, however due to the nature of the design, we were unable to conduct this test.

Objective 3: Design and construct an electromagnetic transducer for the airfoil and bluff body design.

Electrical Calculations

The power output of the electromagnetic transducer depended on several factors. According to Faraday's Law, the electromotive force (emf) is directly proportional to the change in flux and number of turns in the coil, and indirectly proportional to the change in time. In order to increase the emf, the change in flux and turns in the coil should be increased while the change in time is decreased. Below are the equations and variables used to calculate emf for the bluff body in motion.

$$N: \textit{number of turns in coil} = 50$$

$$B: \textit{magnetic field} = 1.23\ \textit{Tesla}$$

$$A: \textit{area perpendicular to the magnetic field} = 0.00049\ m^2$$

$$\Delta\phi : \textit{change in magnetic flux} = B*A \tag{34}$$

$$d: \textit{displacement}$$

$$v: \textit{velocity of magnet}$$

$$\Delta t : \textit{change in time}$$

$$emf = -N\frac{\Delta\phi}{\Delta t} \tag{35}$$

The theoretical emf was calculated for each set of springs as listed in Table 5 below.

Table 5:
Emf for Varying Springs for Bluff Body

Spring Type	**A**	**B**	**C**	**D**
K-value (N/m)	10.5	15.8	38.8	77.1
Velocity (m/s)	0.13	0.72	0.94	1.17
Time in coil	0.16	0.028	0.02	0.017
Emf (mV)	188	1088	1413	1758

As the magnet moved into the coil, the strength of the magnetic field increased in the coil. The current induced in the coil created another field in the opposite direction of the magnet's field to oppose the increase. This is called Lenz's law: when induced magnetic field opposes any change in flux. The negative sign means that the emf created a current and magnetic field that oppose the change in flux.

Using the calculated emf, the theoretical power output was calculated with the following equations and variables. The resistance of the coil was measured with a multimeter.

$$V = voltage$$

$$R = resistance\ of\ coil = 6.773\ \Omega$$

$$P = \frac{V^2}{R} \tag{36}$$

Table 6:
Power Output Calculations for Bluff body

Spring Type	**A**	**B**	**C**	**D**
K-value (N/m)	10.5	15.8	38.8	77.1
Emf (mV)	188	1088	1413	1758
Power (mW)	5.24	174.8	294.6	456.2

Lastly, a load resistance was placed across the output of the rectifier in order to dissipate power. This resistance simulated a load, such as a phone charger. Different resistors were used to

see where the load matched the resistance of the power circuit, which is where maximum power could be dissipated.

Results

In this section, the results of both of the energy harvester designs are discussed. An analysis of the mechanical and electrical aspects of each design is conducted.

Bluff Body Mechanical Results

When testing the bluff body design in the wind tunnel, we used four different springs with a range of k-values to find the spring constant that would generate the largest voltage output. We adjusted the velocity of the wind in the wind tunnel until we were able to find the resonant frequency for each type of spring. We used the resonant frequency because it is the frequency that would allow for the maximum voltage output. Table 7 below shows the results of our bluff body wind tunnel tests.

Table 7:
Bluff Body Wind Tunnel Test Results

Spring Type	**A**	**B**	**C**	**D**
K-value (N/m)	10.5	15.8	38.8	77.1
Wind Speed (m/s)	2.6	2.8	4.0	5.1
Amplitude (m)	0.024	0.016	0.036	0.014
Time per cycle (s)	0.16	0.18	0.08	0.06
Frequency of Bluff Body (Hz)	6.25	5.56	12.5	16.67
Average Bluff Body Velocity (m/s)	0.13	0.72	0.94	1.17

We found that by increasing the spring constants, both the wind speed and bluff body velocity increased.

Using the wind tunnel testing data, the theoretical natural and shedding frequencies of the bluff body were calculated. The measured oscillation frequency for each spring set was calculated from analyzing slow-motion videos of the bluff body in the wind tunnel at its resonant wind speed. The frequency was calculated by observing the period of the oscillations using Equation 37. The theoretical shedding frequency for each spring set was calculated from the actual wind speed at which the bluff body successfully resonated using Equation 38.

$$f_n = \frac{1}{T} \tag{37}$$

T: Period

$$f_s = \frac{25}{22} * V \tag{38}$$

V: Wind Velocity

The measured oscillation frequency and theoretical frequency were similar so we can conclude that the measured oscillation is an accurate representation of the actual natural frequency. Table 8 below shows the comparison of the theoretical and actual values for the natural and shedding frequencies of the bluff body. The theoretical shedding frequency was calculated from the actual wind speed at which resonance occurred.

Table 8:
Comparing Theoretical to Actual Frequency

Spring Constant (N/m)	Theoretical Natural Frequency (TNF) (Hz)	Measured Oscillation Frequency (MOF) (Hz)	Percent Error Between TNF and MOF (%)	Theoretical Shedding Frequency (Hz)
10.5	5.37	6.25	16.4	12.45
15.8	6.57	5.56	15.4	13.74
36.8	10.31	12.5	21.2	19.75
77.1	14.53	16.67	14.7	24.90

We calculated the measured oscillation frequency using slow-motion video to time the period of the oscillations. We calculated the theoretical shedding frequency from the actual wind velocity in the wind tunnel. This is still theoretical because we cannot actually see the vortices to confirm that this calculation was correct. Using the data found through the mechanical wind test, we constructed an electrical system to efficiently harvest power from our device.

Bluff Body Electrical

Initially, we constructed an electromagnetic transducer using silicon diodes; however, the nature of a silicon diode requires a turn-on voltage above our maximum voltage output so we considered other options. We used a capacitor and germanium diodes to construct a bridge rectifier. The rectifier consisted of four diodes, as well as a capacitor to act as a capacitive ballast to reduce noise of the DC output of the rectifier. Our circuit is shown in the figure below.

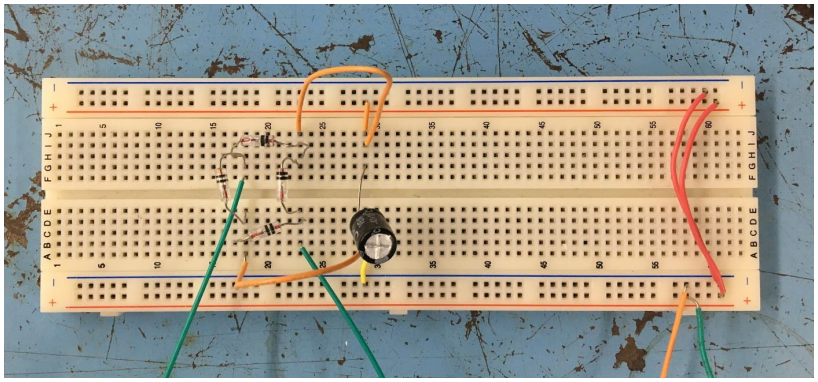

Figure 22: Rectifier

We measured the DC voltage at the output of the rectifier using a multimeter during the wind tunnel tests. We recorded the wind speed that produced the largest open-circuit DC voltage.

Table 9:
Actual DC Voltage at Varying Spring Constants

Spring Type	**A**	**B**	**C**	**D**
K-value (N/m)	10.5	15.8	38.8	77.1
Wind Speed (m/s)	2.6	2.8	4.0	5.1
Emf (mV)	27.1	111	88.5	235

Using these measured DC voltages, we calculated the voltage efficiency based on the calculated theoretical voltages for each spring constant. The theoretical voltages were calculated using Equation 17 shown below. The actual voltage was measured using a multimeter.

$$\varepsilon = -N\frac{d\Phi}{dt}$$

Table 10:
Comparison of Theoretical and Actual Voltage with Efficiency

Spring Constant (N/m)	**Theoretical Voltage (mV)**	**Actual Voltage (mV)**
10.5	189	27.1
15.8	1088	111
36.8	1413	88.5
77.1	1758	235

Using the highest wind speed and strongest suspension springs, we tested different load resistances to find out which load dissipated the most power. Below is Table 11 of the various resistors tested with the resulting power.

Table 11:
Load Dissipated Power

Load (Ohms)	Log Resistance	Voltage (V)	Power (microwatts)
10	1	0.0002	4
51	1.71	0.0015	44.1
200	2.30	0.0048	115.2
300	2.48	0.0064	136.5
1500	3.18	0.026	450.7
2000	3.30	0.03	450.0
5100	3.71	0.058	659.6
10000	4.00	0.081	656.1
20000	4.30	0.106	561.8
30000	4.48	0.125	520.8
43000	4.63	0.139	449.33
51000	4.71	0.142	395.4
100000	5.00	0.167	278.9
200000	5.31	0.184	169.3
300000	5.48	0.19	120.3
5100000	6.71	0.205	8.2

We then graphed the power versus the log of the load resistance. We graphed the log resistance to accurately demonstrate the bell curve. We tested these resistors in order to optimize the load to find the maximum amount of power. The optimal load was found to be between 5,100 and 10,000 Ohms with a resulting maximum output of 659.6 microwatts, as seen in Figure 23

below. These results were expected because the resistance of the coil and rectifier were approximately the same, and power is maximized when load impedance matches the resistance of the power circuit.

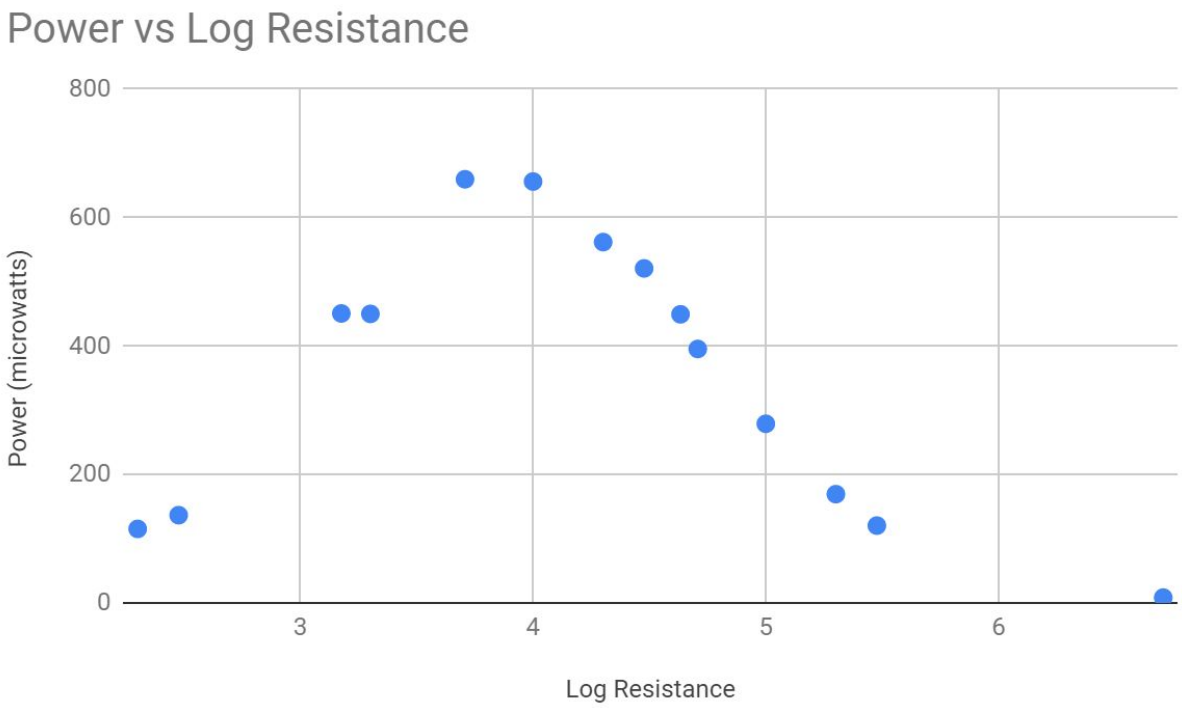

Figure 23: Dissipated Power vs Log Load Resistance

The theoretical maximum power output was estimated to be 456,200 microwatts. The measured maximum power output was estimated to be about 659.6 microwatts. From these measurements, the efficiency of our design was about 0.21%, based on the calculations below.

$$P_T = \frac{1}{2} * \rho * A * U^3$$

$$E = \frac{Actual}{Theoretical} * 100\%$$

$$P_T : Theoretical\ Power$$

$$E : Efficiency$$

Airfoil

When testing the airfoil device in the wind tunnel, we found that two out of the four spring types allowed for the translational and rotational motion of the airfoil. The springs with the lowest and highest k-values did not allow for movement. When using the weakest springs with a k-value of 10.5 N/m, we observed that various wind speeds caused inconsistent movements of the airfoil, because the springs were too weak. When testing the strongest springs with the k-value of 77.1 N/m, the airfoil did not resonate. We can hypothesize that this was due to the lack of lift force.

Table 12:
Airfoil Actual Results

Spring Type	**B**	**C**
K-value (N/m)	14.0	15.8
Wind Speed (m/s)	14.1	15.0
Amplitude (m)	0.13	0.10
Time per cycle (s)	0.09	0.20
Average velocity (m/s)	1.41	0.51
Frequency (Hz)	11.1	5.0
Approximate Emf (mV)	2125	768

When comparing the results of our bluff body system to the airfoil system, we found that the wind velocities required for the airfoil were greater than the bluff body. For the airfoil system to resonate, the wind speed ranged from 14.1m/s to 15.0 m/s. Another difference from the bluff body system was that the airfoil design was not able to self-start. An input force was required for the system to oscillate.

The electromagnetic transducer was not connected to the device due to its instability. With a modified design, the transducer could be mounted. We calculated the approximate

voltage output of the airfoil energy harvester by applying the frequency from the wind test to the calculations used to determine the electrical results of the bluff body energy harvester.

Conclusions and Recommendations

The prototypes were both able to produce VIV oscillations in the wind using the four springs, each having different stiffnesses. The goal of the project was to create a prototype that was a proof-of-concept that could eventually be scaled or modified to be more effective and efficient. The bluff body design was able to move in wind speeds ranging from 2.5 m/s to 6 m/s and the airfoil design was able to move in wind speeds around 15 m/s. The bluff body was able to provide about 660 microwatts of power. This was with a pre-fabricated coil from the voice coil of a speaker. The original bluff body design had an efficiency of 0.21%. Using the highest frequency for the airfoil energy-harvesting device, the power output was estimated to be about 550 microwatts based off of the measurements from the transducer in the bluff body energy-harvesting device.

The bluff body harvester resulted in a difference in the oscillation frequency and the theoretical shedding frequency that seemed to be a factor of two, so the measured wind velocities were higher than the expected wind velocities. We suspected that there were a few different explanations of this phenomenon. First, we thought that the “first mode” of vortex induced vibrations (1:1 ratio of shedding to oscillation frequency) may have not had enough energy at the necessary wind speed to support resonance. This would lend itself to finding another mode of resonance (2:1, 4:1, etc) that requires higher wind speed, and therefore more energy in the swept area. Second, we thought that our Strouhal number might have been inaccurate. Since this number is empirically derived, we were relying on other experimental data. Additionally, this number is calculated using Reynolds number, which may have been different than what we calculated it to be. If the calculated Strouhal number was off by a factor of two, the calculated shedding frequency would be off by a factor of two. This would be possible because of our inability to actually measure the shedding frequency.

The final prototypes functioned as predicted, but the bluff body did not produce enough power to be very useful. This was partly due to the small voltage generated by a magnet and coil

setup that was not optimal for this design creating a small voltage. The fact that the voltage was small directly affected the amount of power we were able to dissipate, and it also prohibited us from using silicon diodes, which have a turn-on voltage of about 0.7 V DC. Because of this, we used germanium diodes, which have a smaller turn-on voltage and a lower efficiency.

A significant problem we faced when developing our airfoil prototype was that the airfoil had separate mechanisms that reacted with each other to produce a complex dynamic movement. This resulted in many unknowns when attempting to solve theoretical spring constants. Our calculations only gave us a general estimate.

We also were unable to attach a transducer to the airfoil design. The movement had a larger amplitude, and due to the nature of our design, it was more complicated to mount an electromagnetic transducer. Additionally, we tested the different spring types used on the bluff body to experimentally find optimal spring constants. However, throughout the testing process, we found that our design would not be feasible in a real-world application, as it required an external force to excite the system, and a high wind speed to sustain it.

A broader problem with our systems was that they all required a semi-consistent wind velocity to operate. The bluff body was more adaptable to changes, but the differences in wind speed were only 1-1.5 m/s, where in natural wind, the velocities would normally fluctuate more.

Potential Improvements

The relatively small output could theoretically be drastically increased by increasing the amount of turns in the coil. It could also be increased by moving the coil closer to the magnet since the magnetic field decays as it moves farther away. We could also increase the efficiency by using a stronger magnet. The airfoil design would have been able to dissipate a similar amount of power after attaching a transducer to the model.

Another way we could increase our power output is by scaling the model up. Scaling up the model would increase the output by increasing the swept area of the bluff body. This would increase the ability of the bluff body to harness energy, because the quantity $E = 1/2 * \rho * A * U^3$ would increase. The force generated by and the momentum of the body would also increase. Because of the increase in force, a significantly larger coil and magnet

could be used. The larger coil and magnet would increase the induced current in the coil, and therefore the opposing magnetic field, but a large assembly could be tuned to take a higher electrical damping force, allowing for more energy to be harnessed.

For a theoretical bluff body weighing 1kg, the resonant frequency would be 5.5 Hz, using springs with spring constants of 300 N/m, and in a flow of air moving 16.5 m/s. This shows that, although the larger swept area of the bluff body would increase the output, the lower frequency could decrease it. Additionally, the larger devices would need to operate in significantly higher wind speeds to resonate at a similar frequency. In order to have an effective and efficient device, the negative and positive aspects of the design would have to be considered.

Implementation Strategy

In order to implement this product, this type of energy has to be viewed by society as a positive and easy alternative that could help economic and social development, as well as the environmental benefits. Through campaigns to promote renewable energy and political support, this will help to change people's and companies' behavior to support and utilize small-scale renewable energy sources in different applications. Some examples of wireless sensor nodes that could be powered by something similar to our device is the Fleck3 which was developed by CSIRO ICT Centre in Australia. The consumption parameters are about 890 microwatts. If we were to implement eight versions of our design, we would be able to generate enough power for the Fleck3 wireless sensor node (Knight, 2008). Additionally, with design modifications, we could improve the efficiency to provide more power.

The most important thing when marketing a new tool is to emphasize the benefits relating to cost and ease of accessibility and manufacturing. Giving users the ability to 3D print all of the parts and offering readily accessible materials such as springs, coils, magnets, and transducers, will help to make the product more successful. With advancement in 3D printing technology, the cost of manufacturing has become more economical.

The ease of accessibility would be achieved by offering the designs online to be 3D printed with detailed instructions on the construction of the assembly. This would encourage companies to use it as it requires minimal effort to print the parts and purchase the additional materials. Additionally, it would be encouraged to have the energy harvesters in series to have a larger power and a more effective use of the harvester. This would also help to attract more customers due to its ability to increase in power output by increasing the quantity of assemblies.

Economically, our design is feasible due to its low cost in materials. If it was mass-produced, the cost of the prototypes would be reduced. Using 3D printing also allows for non-expensive and easy access to the designs, which would help to distribute the energy harvester as long as the user has access to a 3D printer. This would also reduce the shipping costs. The sliders could be 3D printed as long as the user had access to 3D printing in nylon, as our team did not have access to nylon 3D printing. This small and easily accessible design will help to encourage people to take on an easy way to use renewable energy.

Overall, this project demonstrated a proof of concept for our bluff body and airfoil wind energy harvester designs. Based on the lessons learned from this project, we can conclude that with significant improvement in the specifications of the electrical component and further research and development of the airfoil design, a greater efficiency could be achieved. Additionally, scaling the models could also help to improve the efficiencies. Because our results showed the vortex-induced vibrations phenomenon occurring at realistic wind speed conditions, there is potential to use it as a source of energy generation.

References

Abdulmunam, R. T. (2012). Modeling of low power electrostatic wind energy harvester for macro-scale applications *International Journal of Information and Electronics Engineering,* Retrieved from http://ijiee.org/papers/240-L0035.pdf

A'fifah Abdullah Sani, S., Djidjeli, K., & Tang Xing, J. (2016). Geometrical Shape Influence on Energy Harvesting Performance of Oscillating Airfoil. Retrieved from https://eprints.soton.ac.uk/399843/1/Conference Paper_SDC2016.pdf

Barrero-Gil, A. (2010, February 09). Energy harvesting from transverse galloping. Retrieved from https://www.sciencedirect.com/science/article/pii/S0022460X10000891

Bühler, P., Schlaich, P., & Sinner, D. (2018). PDF-Grundlagen. *PDF Bibliothek Der Mediengestaltung,* 2-11. doi:10.1007/978-3-662-54615-4_1

Chatterjee, P. "Aeroelastic-Photovoltaic Ribbons for Integrated Wind and Solar Energy Harvesting." IOP science., http://iopscience.iop.org/article/10.1088/1361-665X/aacbbb/meta.

Corke, T. C., & Thomas, F. O. (2015, January). Dynamic Stall in Pitching Airfoils: Aerodynamic Damping and Compressibility Effects. Retrieved from https://www.annualreviews.org/doi/abs/10.1146/annurev-fluid-010814-013632

Curry, A. (2015, September 02). Wind Industry Plans Serious Changes to Protect Bats. Retrieved from https://news.nationalgeographic.com/energy/2015/09/150902-wind-industry-feathering-to-help-protect-bats/

Diltz, N., Gagnon, J., & Wedell, J. (2017). Vortex induced vibration energy harvesting through piezoelectric transducers Retrieved from https://web.wpi.edu/Pubs/E-project/Available/E-project-042117-160415/unrestricted/VIV_Final_Paper.pdf

Doty, James, et al. "Kármán Vortex Street Energy Harvester for Picoscale Applications." *www.wpi.edu*, Worcester Polytechnic Institute, 2018, Kármán Vortex Street Energy Harvester for Picoscale Applications.

Elliott, A. D. T. (2012). Which is better, electrostatic or piezoelectric energy harvesting systems? *Journal of Physics: Conference Series,* (660) doi:10.1088/1742-6596/660/1/012128

Eveleth, R. (2013, December 16). How Many Birds Do Wind Turbines Really Kill? Retrieved from https://www.smithsonianmag.com/smart-news/how-many-birds-do-wind-turbines-really-kill-180948154/

Giurgiutiu, V. (2014). Piezoelectric materials: Effect of temperature. In R. B. Hetnarski (Ed.), *Encyclopedia of thermal stresses* (pp. 3762-3769). Dordrecht: Springer Netherlands. doi:10.1007/978-94-007-2739-7_327

Hobbs, William B., and David L. Hu. "Tree-Inspired Piezoelectric Energy Harvesting." *Journal of Fluids and Structures*, vol. 28, 2012, pp. 103–114., doi:10.1016/j.jfluidstructs.2011.08.005.

Iqbal, Muhammad. "Hybrid Vibration and Wind Energy Harvesting using Combined Piezoelectric and Electromagnetic Conversion for Bridge Health Monitoring Applications." Science Direct., last modified September 15., https://www.sciencedirect.com/science/article/pii/S0196890418307805.

Jus, Y., Longatte, E., Chaissaing, J., & Sagaut, P. (2014). Low mass-damping vortex-induced vibrations of a single cylinder at moderate reynolds number. *J Press Vessel Technol,* doi:10.1115/1.4027659

Kawamura, T., Nakao, T., Hayashi, M., & Murayama, K. (2001). Flow-Induced Vibration of Bluff Bodies. Strouhal Number Effect on Synchronized Vibration Range of a Circular Cylinder in Cross Flow. *JSME International Journal Series B,44*(4), 729-737. doi:10.1299/jsmeb.44.729

Khan, F. U. (2016). State-of-the-art in vibration-based electrostatic energy harvesting. *Journal of Micromechanics and Microengineering,* doi:10.1088/0960-1317/26/10/103001

Kluger, J., Moon, F., & Rand, R. (2013). Shape optimization of a blunt body Vibro-wind galloping oscillator. *Journal of Fluids and Structures,40*, 185-200. doi:10.1016/j.jfluidstructs.2013.03.014

Knight, C., Davidson, J., & Behrens, S. (2008). Energy Options for Wireless Sensor Nodes. *Sensors,8*(12), 8037-8066. doi:10.3390/s8128037

Kumar, C. N. (2015). Energy collection via Piezoelectricity. *Journal of Physics: Conference Series,662*, 012031. doi:10.1088/1742-6596/662/1/012031

Malleron, K. (2018, February 12). Experimental study of magnetoelectric transducers for

power supply of small biomedical devices. Retrieved September 9, 2018, from https://www.sciencedirect.com/science/article/pii/S0026269217306079

Manmadhan, Aneesh. “Energy Harvesting 'Piezo-Tree' Concept.” *THE HEIGHTS OF TECHNOLOGY*, 29 Apr. 2013, techaneesh.blogspot.com/2013/04/energy-harvesting-piezo-tree-concept.html.

Mccloskey, M. A., Mosher, C. L., & Henderson, E. R. (2017). Wind Energy Conversion by Plant-Inspired Designs. *Plos One,12*(1). doi:10.1371/journal.pone.0170022

Michler, A. (2011, January 20). Vibro-Wind Piezoelectric Pads Harness Wind Energy Without Turbines. Retrieved from https://inhabitat.com/vibro-wind-piezoelectric-pads-harness-wind-energy-without-turbines/

Nabavi, Seyedfakhreddin, and Lihong Zhang. “Portable Wind Energy Harvesters for Low-Power Applications: A Survey.” *Sensors*, vol. 16, no. 7, 2016, p. 1101., doi:10.3390/s16071101.

Orrego, Santiago. "Harvesting Ambient Wind Energy with an Inverted Piezoelectric Flag." Science Direct., last modified May 15, https://www.sciencedirect.com/science/article/pii/S0306261917302350.

Pellegrini, S. P., Tolou, N., & Schenk, M. (2012, May 25). Bistable vibration energy harvesters: A review. Retrieved September 9, 2018, from http://journals.sagepub.com/doi/abs/10.1177/1045389X12444940

P. W. Bearman, “Vortex Shedding from Oscillating Bluff Bodies.” Annual Review of Fluid Mechanics 1984 16:1, 195-222

Şahin, I., & Acir, A. (2015). Numerical and Experimental Investigations of Lift and Drag Performances of NACA 0015 Wind Turbine Airfoil. *International Journal of Materials, Mechanics and Manufacturing, 3*(1), 22-25. doi:10.7763/ijmmm.2015.v3.159

Separation of Flow. (n.d.) *The Great Soviet Encyclopedia, 3rd Edition*. (1970-1979). Retrieved October 9 2018 from https://encyclopedia2.thefreedictionary.com/Separation+of+Flow

Sheldahl, R. E., & Klimas, P. C. (1981). Aerodynamic characteristics of seven symmetrical airfoil sections through 180-degree angle of attack for use in aerodynamic analysis of vertical axis wind turbines. doi:10.2172/6548367

Sirohi, J., & Mahadik, R. (2011, December 28). Harvesting Wind Energy Using a Galloping Piezoelectric Beam. Retrieved September 9, 2018, from https://vibrationacoustics.asmedigitalcollection.asme.org/article.aspx?articleid=1471644

Soti, A. K., Thompson, M. C., Sheridan, J., & Bhardwaj, R. (2017). Harnessing electrical power from vortex-induced vibration of a circular cylinder. *Journal of Fluids and Structures,70*, 360-373. doi:10.1016/j.jfluidstructs.2017.02.009

Subramanian, R. (n.d.). Reynolds Number. Retrieved from https://web2.clarkson.edu/projects/subramanian/ch330/notes/Reynolds Number.pdf

U.S. Energy Information Administration. "U.S. Energy Information Administration - EIA - Independent Statistics and Analysis." *Today in Energy*, www.eia.gov/todayinenergy/detail.php?id=31032.

Varpula, A., Laakso, S. J., Havia, T., Kyynäräinen, J., & Prunnila, M. (2014). Harvesting Vibrational Energy Using Material Work Functions. *Scientific Reports,4*(1). doi:10.1038/srep06799

Wright, I. (2016). Windbeam: An Alternative Approach to Alternative Energy. Retrieved September 9, 2018, from https://www.engineering.com/AdvancedManufacturing/ArticleID/11975/Windbeam-An-Alternative-Approach-to-Alternative-Energy.aspx

Yang, B. (2010). Hybrid energy harvester based on piezoelectric and electromagnetic mechanisms doi://doi.org/10.1117/1.3373516

Zhang, Jiantao. (2017)"A Rotational Piezoelectric Energy Harvester for Efficient Wind Energy Harvesting." Science Direct., last modified Aug 1, https://www.sciencedirect.com/science/article/pii/S0924424717309196.

Zhang, W. (2015, April 25). Geometrical effects on the airfoil flow separation and transition. Retrieved from https://www.sciencedirect.com/science/article/pii/S0045793015001292